



## Application of response surface and Taguchi optimization techniques to air gap membrane distillation for water desalination—A comparative study

Atia E. Khalifa\*, Dahiru U. Lawal

*Mechanical Engineering Department, King Fahd University of Petroleum & Minerals, Dhahran 31261, Saudi Arabia, emails: akhalifa@kfupm.edu.sa (A.E. Khalifa), dahiru@kfupm.edu.sa (D.U. Lawal)*

Received 23 November 2015; Accepted 9 May 2016

---

### ABSTRACT

The performance of an air gap membrane distillation (AGMD) system for water desalination was optimized and compared using Taguchi orthogonal design arrays and the response surface methodology (RSM) Face-Centered Central Composite Design. The variables considered in the optimization are feed flow rate, feed temperature, coolant temperature, coolant flow rate, and air gap width. Additionally, a quadratic RS-model between response and the operating parameters was developed. Analysis of variance was then used to analyze the model and the significant effect of each operating parameter on flux. Results showed that the feed temperature and the air gap width are the most influential factors controlling the permeate production. The sensitivity of the permeate flux to coolant flow rate is marginal compared to other factors. From Taguchi technique, a maximum flux of 76.046 kg/m<sup>2</sup> h was obtained at optimum conditions. The RSM approach produced a maximum flux of 76.998 kg/m<sup>2</sup> h at optimum conditions. Although both techniques predicted very similar results, the RSM gives better predictions of the influence of operating parameters on response, and it is a better tool for the optimization of AGMD system compared to Taguchi methodology.

*Keywords:* Water desalination; Membrane distillation; Performance optimization; Response surface methodology; Taguchi methodology; Comparative study

---

### 1. Introduction

Shortage or non-availability of potable/fresh water is one of the basic challenges faced by modern societies. Many countries in the world, especially those in arid areas face the problem of water shortage. To overcome the shortage of freshwater, the world today depends on desalination of seawater and brackish water [1,2]. About 18,426 desalination plants are currently in operation all over the world. These plants are responsible for the production capacity of about

86,600,000 m<sup>3</sup> of freshwater per day [3]. Most conventional desalination plants are thermally based, while the number of membrane-based plants, such as reverse osmosis, is increasing worldwide.

Membrane technologies are growing for water desalination and treatment applications. Membrane distillation (MD) is one of those technologies that have a potential and can be applied to separate water vapor from seawater and brackish water. Vapor separation takes place inside the MD module which usually consists of feed and coolant compartments, separated by micro-porous hydrophobic membrane. The volatile compounds in the hot feed stream evaporates, and

---

\*Corresponding author.

permeates in vapor phase across the membrane pores to the cooling side of the membrane where the vapor condenses either inside or outside the MD cell. Other than seawater desalination, MD process can also be employed in applications including wastewater treatment, pharmaceutical and textile industries [4,5], removal of volatile organic compounds from contaminated drinking water [6–8], and concentration of aqueous solution such as fruit juice [9–11]. Among numerous benefits of MD process is the ability to operate the MD system with feed streams at temperatures far below the boiling point. Unlike other thermally based desalination processes, MD requires only heating, and not boiling the feedwater [12].

The direct contact MD, air gap MD, vacuum MD, and sweeping gas MD are the main MD design configurations [12,13]. Both direct contact membrane distillation (DCMD) and air gap membrane distillation (AGMD) have drawn fair attention of many MD investigators. Some researchers have also investigated another MD design configuration known as liquid gap membrane distillation (LGMD) [14–16]. Replacing the stagnant air in the air gap of AGMD with water is reported to have improved the system flux by about 140% [14]. One advantage of AGMD process is the system provisions to use any type of coolant as the cooling solution, since the coolant does not, in any way, come in direct contact with the condensate distillate. In the AGMD, the established vapor pressure difference due to the temperature difference between the sides of the membrane induces evaporation of water from the hot feed stream. The water vapor diffuses across the membrane pores, and then across the stagnant air gap staged between the membrane surface and the cooling surface. The vapor condensed on reaching the cooling surface to form distilled water; which can be then withdrawn from the air gap out of the module [17].

Several studies addressed the performance of AGMD system for water desalination. Bahar et al. [18] designed a unique condensation surface that allows the manipulation of mass transfer by enhancing the heat transfer during condensation. Their results showed that a special cooling plate design having number of fins enhances the system performance by about 50% when compared to a flat cooling plate. Tian et al. [19] presented an innovative module design which allows partial contact of membrane material with the condensation surface. The design minimized the additional transport resistance established by the air gap, thereby improving the efficiency of the system. With 77°C feed temperature, and coolant temperature of 10°C, an impressive flux of 119 kg/m<sup>2</sup> h was reported. Geng et al. [20] presented a new design of

AGMD process, equipped with internal latent-heat-recovery. They obtained a maximum permeate flux of 5.30 kg/m<sup>2</sup> h, and attained a very high gained output ratio of 5.7. In addition, they introduced vapor pressure polarization coefficient to evaluate the effective vapor pressure difference for the transport.

Attempts have been made by various researchers toward commercialization of MD systems. Burrieza et al. [21] analyzed the performance of two different pre-commercial air gap membrane desalination modules, which were developed by the Singaporean enterprise Keppel Seghers, and tested under actual conditions intermittently for about 2,400 h during two years. The system was directly coupled with a static collector solar field. One module consisted of three stages connected in series, and the other module was a single-stage design. The feed solution had concentration ranging from 1 to 35 g/L. The obtained distillate conductivity ranged from 2 to 5  $\mu\text{S}/\text{cm}$ . For the single-stage module, the minimum specific thermal energy consumption was found to be 1,805 kWh/m<sup>3</sup>, while that for the multi-stage module was found to be 294 kWh/m<sup>3</sup>. Winter et al. [22] presented experimental studies on full-scale spiral-wound MD-modules. Fully automated performance test facility, module technology, module fabrication, and the characterization procedures were discussed in their work. About 130 modules were fabricated and characterized in special automated test facilities. The obtained distillate ranged between 10 and 25 kg/h, with a specific energy consumption of 130–207 kWh/m<sup>3</sup>. The reported product conductivity was about 3.5  $\mu\text{S}/\text{cm}$  at maximum. Aguirre et al. [23] evaluated two different modules using spiral-wound membranes. The module used solar energy as the feed source. The analysis was conducted at Plataforma Solar de Almeria, Spain. Different commercial modules and real-scale prototypes were tested in continuous operation. One of the module was a liquid-gap configuration (LGMD), while the other was an air-gap configuration (AGMD). The gain output ratio for the LGMD was found to be three while that of AGMD was found to be seven. However, AGMD was found to produce lower distillate fluxes as compared to LGMD. The AGMD configuration provided lower product quality. Both the configurations were found to have similar recovery ratios.

The significant factors controlling the performance of AGMD system have been recognized. To improve the productivity of AGMD system, these controlling factors (such as feed temperature, feed flow rate, etc.) should be optimized. In the past, the usual optimization techniques for a system was mainly single variable dependent, with other variables kept fixed [24]. This kind of optimization approach demands a huge

number of experimental runs. Moreover, data needed to correlate the objective function and decision variables can hardly reflect the interaction of the multi-variable dependent process. Naturally, the most accurate conventional way to optimize the system is to try out all possible conditions, and compare the objective functions to identify the optimized match. However, this type of approach is time-consuming and inefficient, especially for some complicated problems of multi-variables with a large value domain that required high accuracy [25].

## 2. Design of Experiment (DoE)

Statistical optimization approaches (such as, response surface methodology (RSM), Taguchi technique, and factorial design) are known as Design of Experiment (DoE) and are now widely used in place of one-factor-at-a-time experimental approach, due to the aforementioned setbacks.

Taguchi design is a fractional factorial design matrix [26], which has been widely used to optimize design variables. This method can significantly reduce the overall experimental cost and testing time. Taguchi methodology has shown that there is no need to run full factorial experiments if one can carefully select the experimental runs. Compared to other DoE techniques, Taguchi method allows obtaining experimental results using fewer experimental runs and offers a simple and systematic approach to optimize the performance and quality [27,28]. The optimization process using Taguchi methodology can be classified into four phases; planning, conducting, analysis, and validation, and each phase has a separate objective and contributes towards the overall optimization process [29]. Orthogonal array (OA) and the signal-to-noise ratio (S/N ratio) are the two major tools used in Taguchi design. The OA is a matrix of numbers arranged in rows and columns, selected from all possible combinations of the controllable factors. For instance,  $L_{27} (3^5)$  orthogonal design matrix means that 27 experiments are to be conducted to study 5 variables at 3 levels each. Signal-to-noise ratio is the ratio of sensitivity to variability. By minimizing the effect of noise factor, we are actually maximizing S/N ratio, thereby improving the product quality. Depending on the objective function, S/N ratio may be classified as smaller is the best, nominal is the best, and larger is the best characteristics. In this study, “the larger is the best characteristic” is considered; because we need a maximum permeate flux. For Larger-is-Better situation, S/N ratio may be estimated as [30]:

$$S/N = -10 \log_{10} \left[ \sum_i \left( \frac{1}{y_i} \right)^2 \frac{1}{n} \right] \quad (1)$$

where  $y_i$  is the response at each observation and  $n$  is the number of observations.

Taguchi methodology has been utilized successfully to optimize different MD systems. Mohammadi and Safavi [30] used Taguchi methodology to optimized vacuum membrane distillation system for water desalination. The results obtained showed that the feed temperature of 55°C, feed flow rate of 30 mL/s, feed concentration of 60 g/L, and vacuum pressure of 30 mbar are the optimum factors level, which produce the optimum flux of 16.96 kg/m<sup>2</sup> h. Khalifa and Lawal [31] optimized the performance of an AGMD system for water desalination using Taguchi methodology. Mohammadi and Kazemi [26] employed Taguchi techniques to treatment the phenolic wastewater using vacuum membrane distillation. A maximum flux of 109.257 kg/m<sup>2</sup> h was reached at the optimum feed temperature of 65°C, pH of 12.5, feed concentration of 510 mg/L, and vacuum pressure of 60 mbar. While at the optimum feed temperature of 45°C, pH at 13, feed concentration of 1,000 mg/L, and vacuum pressure of 60 mbar, they reached an optimum separation factor of 63.635.

RSM is a collection of statistical and mathematical techniques used for developing, improving, and optimizing processes. It is used to examine the relationship between one or more response variables, and a set of quantitative experimental variables. It is a sequential experimentation strategy for building and optimizing a model [32–34]. In the RSM, the regression technique, based on least square method, is used to estimate the regression coefficient. RSM also quantifies the relationships between the controllable input parameters and the obtained response surface [28,35]. The RSM method permits different choice of designs like; Central Composite Design (CCD), Box–Behnken design, one factor design, and Miscellaneous designs. However, the most widely used RSM designs are the CCD, and the Box–Behnken design.

The CCD designs are recommended when employing sequential experimentation, because these designs can incorporate information from a properly planned factorial experiment. Furthermore, CCD provides efficient estimation of the quadratic terms in the second-order model. On the other hand, Box–Behnken design is used when conducting non-sequential experiments (when planning to perform the experiment once). The design also allows efficient estimation of the first and second-order coefficients. More insight into CCD and

Box–Behnken design can be found in the reference [36]. In this study, the Face-Centered Central Composite Design (FCCD) was used, since it is employed when the domain of operation encloses the full region of interest described by the variable ranges. It is the least prone to corruption due to sources of experimental error associated with setup and operation, and it is the simplest variety of CCD since it requires only three levels of each experiment variable [33].

RSM has been used effectively to optimize MD systems by different researchers. Mohammadi et al. [37] used RSM method to optimized vacuum membrane distillation system for water desalination. The design matrix adopted was Box–Behnken design. At the feed temperature of 55°C, feed flow rate of 38.63 mL/s, feed concentration of 100 g/L, and vacuum pressure of 10 mbar, an optimum system flux of 17.96 kg/m<sup>2</sup> h was recorded. Khayet and Cojocaru [38] modeled and optimized AGMD system using RSM method. The specific performance index and performance index were calculated using the developed regression model, with the effect of energy consumption as function of different operating variables. Statistical analysis was performed using analysis of variance (ANOVA) to determine the significant level of each parameter. Using Monte Carlo simulation, an optimum variable combination for performance index was 71°C feed inlet temperature, 13.9°C cooling inlet temperature and 183 L/h feed flow rate. This combination gave an optimum experimental permeate flux of 47.189 kg/m<sup>2</sup> h. Khayet et al. [39] also applied RSM method to investigate the effect of feed temperature, coolant flow rate, feed flow rate, and feed concentration in DCMD. A regression model was developed and then validated against the experimental findings. Results showed a good agreement between the developed model and the experimental results. An algorithm was subsequently developed by exploring response surface in the valid region of operating conditions. Gradient method was used to determine the optimal points in the region of experimentation for different membrane sheets. The optimum conditions were found to be dependent of the membrane material, type, and properties.

Investigators have utilized RSM and Taguchi techniques to optimize some MD systems. However, to the best of authors' knowledge, no work has been done to ascertain which of the two techniques gives better insights into the significant effect of controlling parameters on the MD response. It is also not clear which DoE tool is better for MD process optimization. The influence of air gap thickness, which is one of the most important AGMD process controlling parameter had not been given its due attention in previous

studies of any of the aforementioned statistical optimization approaches.

The objective of the current work is to apply and compare the optimization of AGMD system for water desalination, using the RSM and Taguchi technique. Experimental investigation of the significant influence of operating parameters on the system performance is necessary prior to the application of optimization techniques. The variable parameters under consideration are: feed temperature, coolant temperature, feed flow rate, coolant flow rate, and air gap width.

### 3. Experimental investigation of performance variables

#### 3.1. Experimental setup

An experimental lab-scale setup was constructed with a channeled AGMD module, which includes a flat sheet membrane, to investigate the MD system performance under different ranges of the main operating conditions. Fig. 1 shows the experimental setup and its schematic, while Fig. 2 shows the details of the AGMD module and its assembly. The feedwater is heated to the required temperature using a thermostat water circulation bath and is pumped to the membrane cell (module) using a small centrifugal pump. The hot feed passes over the hydrophobic membrane surface and returns back to the feed container. Coolant water temperature is controlled and its flow is circulated using a refrigerated water bath circulator. The air gap width is determined by the thickness of the spacer and rubber gaskets installed between the membrane and the condensation plate; as shown in Fig. 2. Condensation takes place on the surface of the 1.5 mm-thick brass plate. The module three channels were machined from Plexiglas material using CNC machine. The dimensions of each channel are 22 mm width, 6 mm depth, and length of 66 mm. The effective membrane permeation area is  $2.29 \times 10^{-3} \text{ m}^2$ .

Thermocouples and pressure gauges were used to monitor the inlet and outlet temperatures and pressures for feed and coolant waters; respectively. Water flow rates at the inlet of both feed side and coolant side of the MD module were controlled using control valves, and monitored with flow meters with display. The volumes of the collected distillate and the samples time were measured for each experiment after the system reached thermal steady-state conditions such that repeating the measurements under the set operating conditions results in the same permeate flux. Permeate flux was then calculated and reported in units of kg/m<sup>2</sup> h. The concentrations of the feed inlet water and the collected distillate were measured using

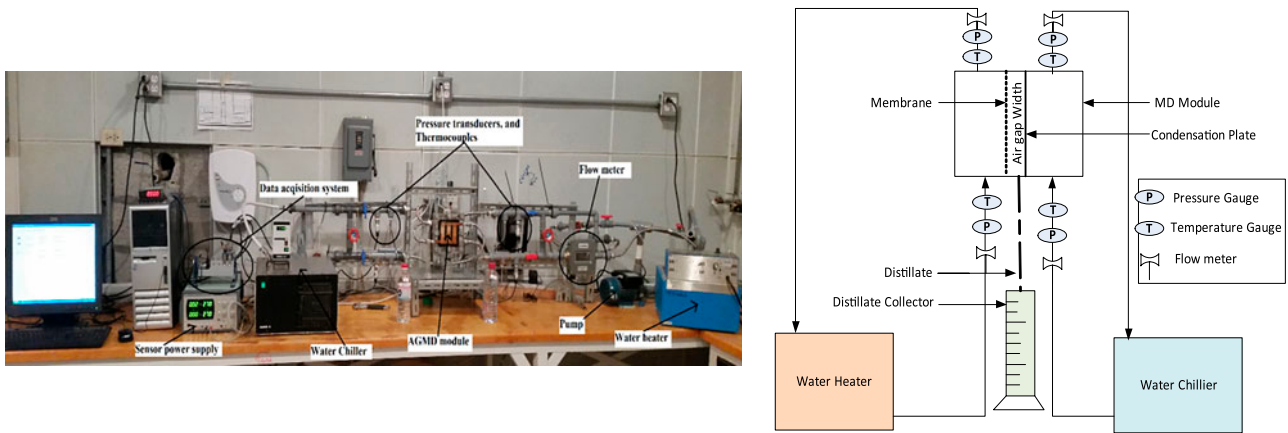


Fig. 1. The experimental setup—a photo of actual setup and its schematic representation.

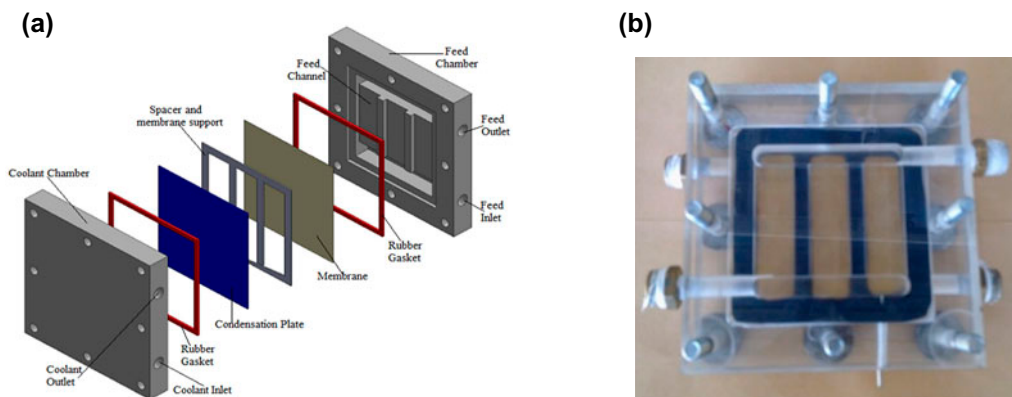


Fig. 2. Details of the AGMD module: (a) An exploded view of the AGMD module assembly and (b) The assembled AGMD module.

a calibrated conductivity meter. The measured total dissolved solids (TDS) of feed solution is 4,060 mg/L, which is fixed supply for all experiments and thus the effect of feed concentration is not considered as a variable in the present work.

The membrane used is a commercial polytetrafluoroethylene composite sheets with 0.45 μm mean pore size. The membrane sheets have an active Teflon layer and a support layer. In order to determine the membrane parameters, various characterization techniques are employed. The actually measured membrane properties in our lab are listed in Table 1.

### 3.2. Experimental results

Prior to data generation for statistical scrutiny, a parametric experimental investigation was conducted to study the influence of operating and design variables on the AGMD performance, and to determine the domain (range) of each variable to be considered

Table 1  
Characteristics of the used PTFE membranes

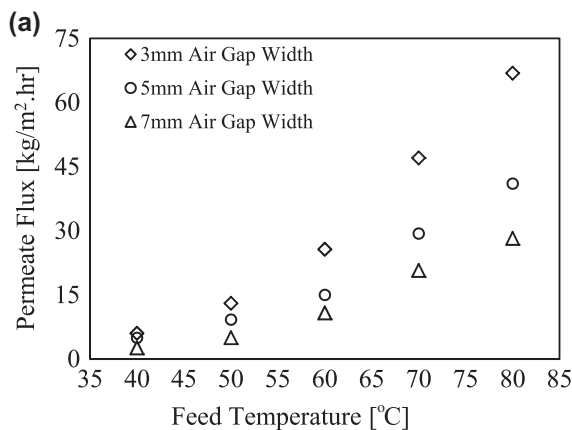
Property	Value
Type	PTFE (commercially 0.45 μm)
Manufacturer	Tisch Scientific Company
$\delta_{full,membrane}$ (μm)	153.9 ± 13.6
$\delta_{active,teflon}$ (μm)	6.9 ± 2.0
$\delta_{support}$ (μm)	141.4 ± 15.8
$d_p$ (nm)	379 ± 8
$\epsilon$ (%)	79.7 ± 8.7
$\tau$ (tortuosity)	$\tau = (1/\epsilon) = 1.25$
$\theta$ (°) active layer	139.0 ± 2.8
$\theta$ (°) support layer	119.3 ± 1.0
LEP (bar)	2.4 ± 0.1 (distillate water) 2.6 ± 0.1 (salinity 30 g/L)

Notes: ( $\delta_{full,membrane}$ : membrane thickness,  $\delta_{active}$ : thickness of membrane active layer,  $d_p$ : mean pore size,  $\epsilon$ : porosity,  $\theta$ : water contact angle, LEP: liquid entry pressure).

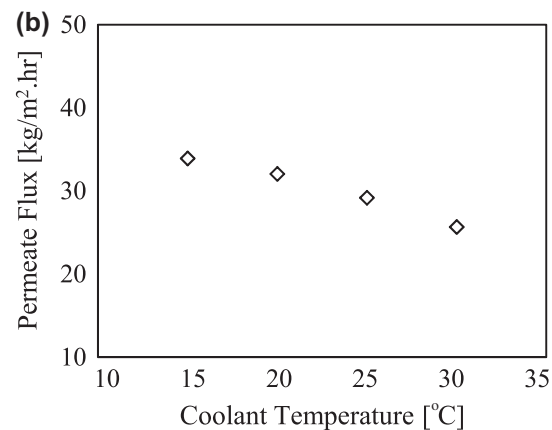
in the optimization process. The influences of feed temperature, coolant temperature, feed flow rate, coolant flow rate, and air gap width on the permeate flux are measured. The considered parameters are the main influencing ones for any AGMD system, excluding the membrane type. The results of the experimental investigation are portrayed in Fig. 3(a)–(d). For consistency, the specific experimental conditions are given below each figure.

It can be observed from Fig. 3(a) that increasing the feed temperature encourages the water evaporation, and increases the vapor pressure in the feed channel exponentially that consequently increases the permeate flux in an exponential manner. The exponential rise in flux is due to the exponential relationship between the vapor pressure and temperature as given

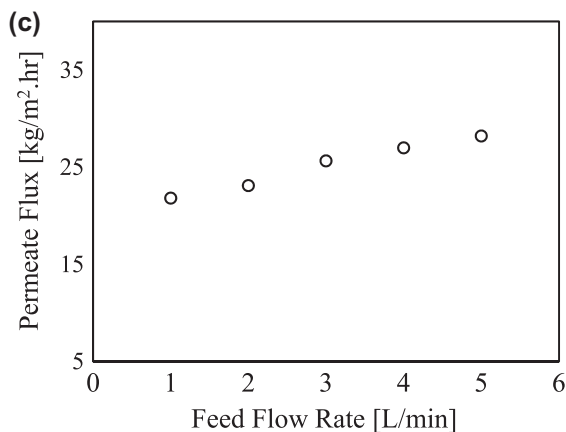
by Antoine equation [12]. The effect of the gap width is included in Fig. 3(a) for constancy and comparison purposes. The flux was observed to decrease with increasing air gap width. For instance, with an air gap width of 3 mm, increasing the feed temperature from 40 to 80°C leads to about 1,000% increase in flux (from 6 to 66 kg/m<sup>2</sup> h). Similarly, for the same range of feed temperature, flux increases by 720–965% for air gap widths of 5–7 mm, respectively. This is because decreasing the air gap width reduces the resistance to mass diffusion of the vapor molecules across the air gap and increases the temperature gradient within the gap, leading to higher permeate flux. The flux was observed to increase by a constant percentage of 135% when the air gap width reduced from 7 to 3 mm, at feed temperatures of 40, 60, and 80°C.



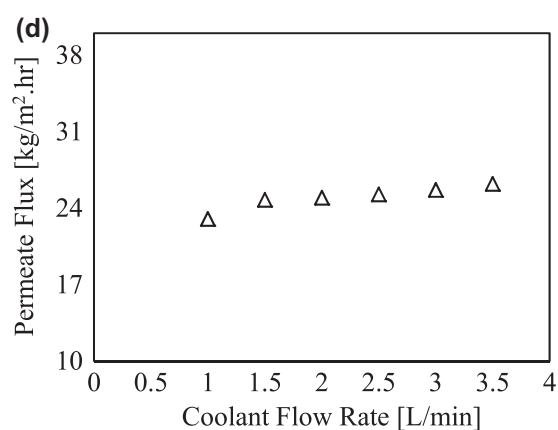
Test Conditions: Coolant temperature of 30°C, feed flow rate of 3 l/min, and coolant flow rate of 3 l/min.



Test conditions: Feed temperature of 60°C, feed flow rate of 3 l/min, coolant flow rate of 3 l/min, and air gap width of 3mm.



Test conditions: Feed temperature of 60°C, Coolant temperature of 30°C, coolant flow rate of 3 l/min, and air gap width of 3mm.



Test conditions: Feed temperature of 60°C, Coolant temperature of 30°C, feed flow rate of 3 l/min, and air gap width of 3mm.

Fig. 3. Effect of AGMD operating parameters on permeate flux: (a) Effect of feed temperature and air gap width on flux, (b) Effect of coolant temperature on flux, (c) Effect of feed flow rate on flux, and (d) Effect of coolant flow rate on flux.

Decreasing the coolant temperature increases the transmembrane potential, enhances the condensation process, and leads to increase in permeate flux as seen in Fig. 3(b). However, this does not increase the vapor production in the hot feed channels. Under the test conditions shown in Fig. 3(b), about 32% increase in flux was achieved when the coolant temperature was reduced from 30 to 15°C. Fig. 3(c) shows that flux increases with increasing feed flow rate because of higher turbulence levels and enhanced mixing in the boundary layer adjacent to the membrane surface. Increasing the feed flow rate from 1 to 5 L/min resulted in about 30% increase in the permeate flux due to better heat and mass transfer coefficients and less effects of temperature polarization across the membrane. The sensitivity of permeate flux to coolant flow rate is presented in Fig. 3(d). The coolant flow rate has less impact on flux with about 13% increase in flux when increasing the coolant flow rate from 1 to 3.5 L/min.

In conclusion of this section, the most significant variables affecting the performance of the AGMD system are actually the feed temperature and the air gap width. To less extent, the feed flow rate and coolant

temperature have clear effects on the system flux. The lesser impact on flux is for the coolant flow rate. It worth mentioning that the TDS of the collected permeate ranged between 4 and 10 mg/L, with a corresponding salt rejection factor ranging between 99.9 and 99.75%, which indicates the ability of the AGMD system to produce very high quality distillate.

#### 4. Optimization

The ranges and the operating conditions considered for the AGMD system optimization were selected based on the experimental investigations presented in Section 3 and results shown earlier in Fig. 3. Since the system flux is significant for feed temperature range between 60 and 80°C, the three levels considered for the feed temperature are 60, 70, and 80°C. In addition, three levels for feed flow rate, coolant temperature, coolant flow rate, and air gap width were selected to cover wide range for each variable along with the experimental practicality. For coolant temperature, the selected values are 20, 25, and 30°C, which can be achieved easily in the lab environment and may require no

Table 2  
Taguchi L<sub>27</sub> (3<sup>5</sup>) orthogonal design matrix and the responses [27]

Run	Feed temp. (°C)	Coolant temp. (°C)	Feed flow rate (L/min)	Coolant flow rate (L/min)	Air gap (mm)	Flux (Averaged) (kg/m <sup>2</sup> h)	S/N ratio (dB)
1	60	20	1	1	3	25.1211	28.0005
2	60	20	1	1	5	16.049	24.1077
3	60	20	1	1	7	12.0037	21.5856
4	60	25	3	2	3	26.6469	28.5125
5	60	25	3	2	5	16.6195	24.4121
6	60	25	3	2	7	12.1224	21.6704
7	60	30	5	3	3	26.7095	28.5332
8	60	30	5	3	5	16.6426	24.4242
9	60	30	5	3	7	12.1735	21.7008
10	70	20	3	3	3	53.0461	34.493
11	70	20	3	3	5	34.9911	30.879
12	70	20	3	3	7	27.8864	28.9075
13	70	25	5	1	3	58.2577	35.3068
14	70	25	5	1	5	35.1097	30.9085
15	70	25	5	1	7	23.3961	27.3797
16	70	30	1	2	3	37.7657	31.5418
17	70	30	1	2	5	23.5857	27.4528
18	70	30	1	2	7	17.1866	24.7036
19	80	20	5	2	3	76.0457	37.6212
20	80	20	5	2	5	49.0294	33.8091
21	80	20	5	2	7	36.088	31.1472
22	80	25	1	3	3	61.5822	35.7891
23	80	25	1	3	5	38.4178	31.6903
24	80	25	1	3	7	28.3996	29.0491
25	80	30	3	1	3	64.181	36.1481
26	80	30	3	1	5	38.4759	31.7031
27	80	30	3	1	7	27.2184	28.697

external cooling (range of energy saving). The selected values of feed flow rate are 1, 3, and 5 L/min, and the selected values for coolant flow rate are 1, 2, and 3 L/min. Three air gap widths of 3, 5, and 7 mm are considered in the optimization. Considering the aforementioned conditions and variable ranges, the optimization of the AGMD system is carried out using both Taguchi method and RSM and is then compared.

#### 4.1. Taguchi technique

Details of the application of Taguchi methodology to the AGMD system, using Minitab software, is explained by Khalifa and Lawal [27]. Table 2 presents the Taguchi orthogonal design matrix  $L_{27} (3^5)$  for the selected five factors at the selected three levels for each factor. Twenty-seven experimental runs were conducted with four repetitions for each run to observe the effects of uncontrollable factors (S/N ratio) on this process. The response (permeate flux) for different combinations is shown with the signal-to-noise ratio (S/N).

The optimum experimental value of permeate flux is  $76.0457 \text{ kg/m}^2 \text{ h}$  which was obtained at the feed temperature of  $80^\circ\text{C}$ , coolant temperature of  $20^\circ\text{C}$ , feed flow rate of 5 L/min, coolant flow rate of 2 L/min, with air gap width of 3 mm. The variation in the individual response of the five controlling parameters, represented by the main effect plots for permeate flux

and S/N ratio, are shown in Figs. 4 and 5. Increasing the feed temperature resulted in a continuous increase in the values of permeate flux and S/N ratio. Operating the AGMD module at a higher temperature yields a higher system flux. The permeate flux and the S/N ratio decrease with increasing the coolant temperature and the air gap width. Increasing the feed flow rate enhances the system flux and increased the S/N ratio, because of the higher turbulence level generated in the feed channels. Coolant flow rate shows insignificant effect on permeate flux and S/N ratio.

To evaluate the relative importance of each factor on the permeate flux, the ANOVA was applied at 95% confidence level (level of significant  $\alpha = 0.05$ ). The ANOVA analysis of responses is shown in Table 3. All factors have significant effect on the response except the coolant flow rate. The  $p$ -values of feed temperature, coolant temperature, feed flow rate, and air gap width ( $p$ -values  $< 0.05$ ) indicate that all the four operating factors significantly influence the system performance. However, the  $p$ -value of coolant flow rate is 0.972, which is greater than 0.05 confidence level. Hence, the coolant flow rate is statistically not a significant factor. Another way to determine and rank the order of significance of each factor is with the help of  $F$ -value and sum of square. Factors with the largest  $F$ -values are the most influential parameters [25]. Thus, feed temperature and air gap width provide the largest contribution to the total sum of squares, and

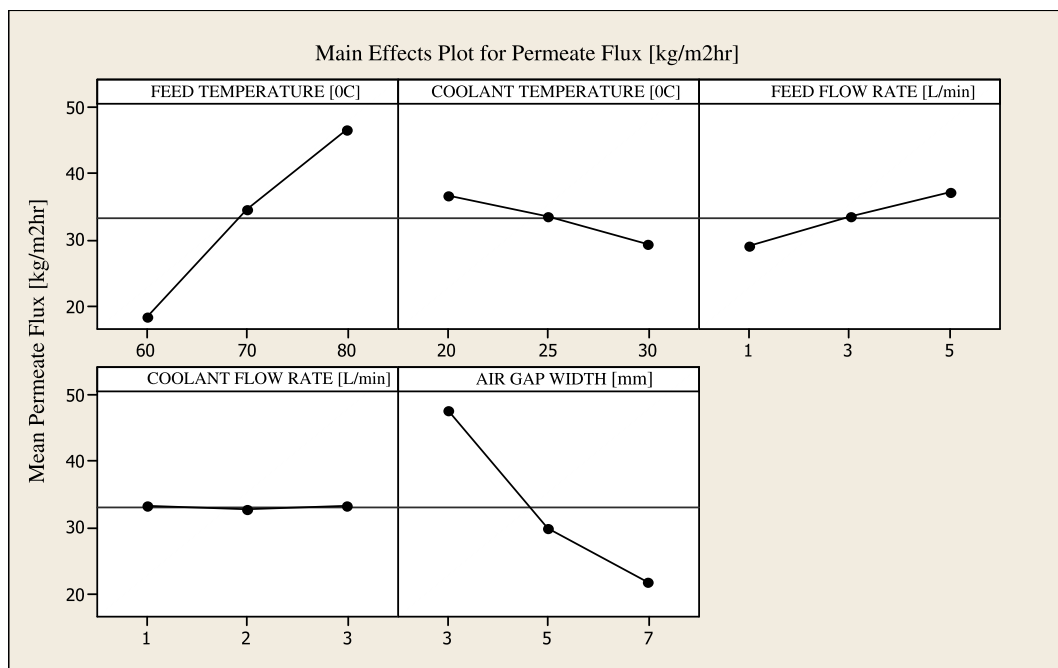


Fig. 4. AGMD Main effect plot for mean permeate flux [27].

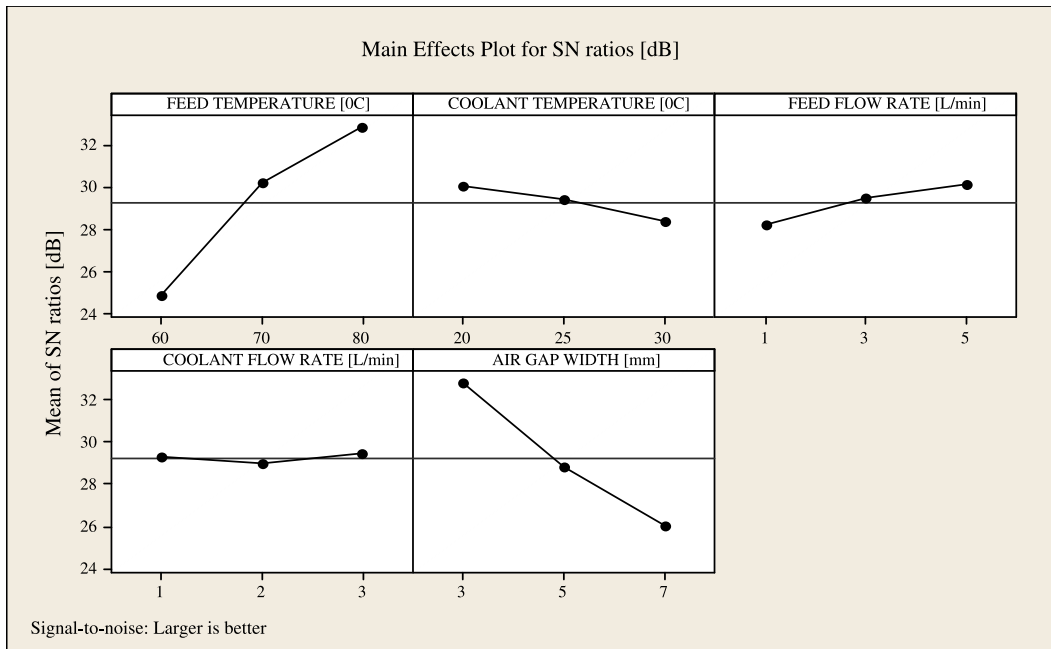


Fig. 5. AGMD Main effect plot for mean signal-to-noise ratio [27].

Table 3  
Analysis of variance for responses, using adjusted SS [27]

Source	df	Seq. SS	Adj. SS	Adj. MS	F	p
Feed temperature	2	3,650.47	3,650.47	1,825.24	61.91	0.000
Coolant temperature	2	245.25	245.25	122.62	4.16	0.035
Feed flow rate	2	300.26	300.26	150.13	5.09	0.019
Coolant flow rate	2	1.66	1.66	0.83	0.03	0.972
Air gap width	2	3,156.36	3,156.36	1,578.18	53.53	0.000
Residual error	16	471.71	471.71	29.48		
Total	16	7,825.71				

Notes: S = 5.430, R<sup>2</sup> = 94.0%, R<sup>2</sup> (adj.) = 90.2%.

correspondingly have the strongest effects on system flux.

The best regression model for calculating the permeate distillate production is given by [27]:

$$\begin{aligned}
 J = & -197.79 + 5.8611 A - 0.7369 B + 2.0372 C \\
 & + 1.1218 D - 0.02162 A^2 + 1.2220 D^2 \\
 & - 0.28302 A \times D
 \end{aligned}
 \tag{2}$$

where *J* is the calculated permeate flux (kg/m<sup>2</sup> h), *A* is the feed temperature (°C), *B* is the coolant temperature (°C), *C* is the feed flow rate (L/min), and *D* is the air gap width (mm). Note that Eq. (2) is valid only in the range of the optimized variables.

#### 4.2. Response surface methodology (RSM) analysis

According to FCCD matrix, a total number of 50 experimental runs were conducted. The RSM design layout and the response for FCCD option are presented in Table 4, with the permeate flux as the selected response. Fig. 6 shows the excellent match between experimental and predicted responses for square root of permeate flux. The results obtained from the experiments conducted according to RSM design layout were used into statistical design software “Design-Expert” for further analysis. The nature and the range of the obtained experimental data demanded transformation because the ratio of maximum to minimum response is greater than 10. Furthermore, a square root transformation was

Table 4  
Experimental data for FCCD of the five variables at three levels

Exp. run	Type	Feed temp. (°C)	Coolant temp. (°C)	Feed flow rate (L/min)	Coolant flow rate (L/min)	Air gap (mm)	Experimental flux (kg/m <sup>2</sup> h)	Predicted permeate flux (kg/m <sup>2</sup> h), Eq. (3)
1	Fact	80	30	5	1	3	68.02441	67.32162624
2	Fact	60	20	5	1	7	21.14541	21.08252608
3	Fact	80	30	5	1	7	30.82769	30.48691035
4	Axial	70	30	3	2	5	29.24173	28.56040096
5	Axial	70	25	3	2	3	50.75248	50.57827743
6	Fact	80	30	1	3	3	61.47963	61.37739247
7	Fact	80	20	1	1	7	30.04775	29.86443032
8	Fact	60	30	5	1	7	13.77635	13.3479183
9	Fact	60	30	1	1	7	5.62735	6.214551906
10	Axial	70	20	3	2	5	36.61079	36.73556463
11	Fact	80	20	1	3	7	31.65197	31.58003678
12	Center	70	25	3	2	5	32.92626	32.51953442
13	Fact	60	30	5	1	3	28.33139	27.95702916
14	Fact	60	20	1	1	7	12.99641	12.69742046
15	Center	70	25	3	2	5	32.92626	32.51953442
16	Center	70	25	3	2	5	32.92626	32.51953442
17	Fact	60	30	5	3	7	15.38057	14.50281605
18	Fact	80	20	5	1	3	75.39347	73.41267691
19	Center	70	25	3	2	5	32.92626	32.51953442
20	Fact	60	20	5	3	3	37.30467	37.2790938
21	Fact	80	30	1	1	3	59.87541	58.9762024
22	Axial	70	25	5	2	5	37.00076	37.1001805
23	Center	70	25	3	2	5	32.92626	32.51953442
24	Fact	80	30	1	3	7	24.28291	23.51734085
25	Fact	60	30	5	3	3	29.93561	29.61772261
26	Fact	80	20	5	1	7	38.19675	37.93680649
27	Fact	60	30	1	1	3	20.18239	19.60970538
28	Fact	80	30	5	3	3	69.62863	69.88544849
29	Center	70	25	3	2	5	32.92626	32.51953442
30	Fact	60	20	1	3	3	29.15567	28.93210908
31	Fact	80	20	5	3	7	39.80097	39.86738147
32	Fact	80	20	1	3	3	68.84869	69.38672422
33	Fact	60	20	1	3	7	14.60063	13.82441633
34	Axial	70	25	3	1	5	32.12415	31.64289923
35	Center	70	25	3	2	5	32.92626	32.51953442
36	Axial	70	25	3	2	7	24.8766	24.40094877
37	Axial	70	25	3	3	5	33.72837	33.40814741
38	Center	70	25	3	2	5	32.92626	32.51953442
39	Fact	60	30	1	3	3	21.78661	21.00444538
40	Fact	60	20	5	1	3	35.70045	35.4130299
41	Axial	70	25	1	2	5	28.85176	28.24059994
42	Fact	60	20	5	3	7	22.74963	22.52781174
43	Axial	60	25	3	2	5	16.57773	17.24899091
44	Fact	60	30	1	3	7	7.23157	7.01018979
45	Axial	80	25	3	2	5	44.94991	43.06908182
46	Fact	60	20	1	1	3	27.55145	27.29102856
47	Fact	80	20	1	1	3	67.24447	66.8321521
48	Fact	80	30	1	1	7	22.67869	22.04013391
49	Fact	80	30	5	3	7	32.43191	32.22005587
50	Fact	80	20	5	3	3	76.99769	76.08891114

Notes: Axial: the axial points, also known as star points, let you estimate curvature.

Center: the central points, replicated to provide an estimate of experimental error variance.

Fact: the factorial points.

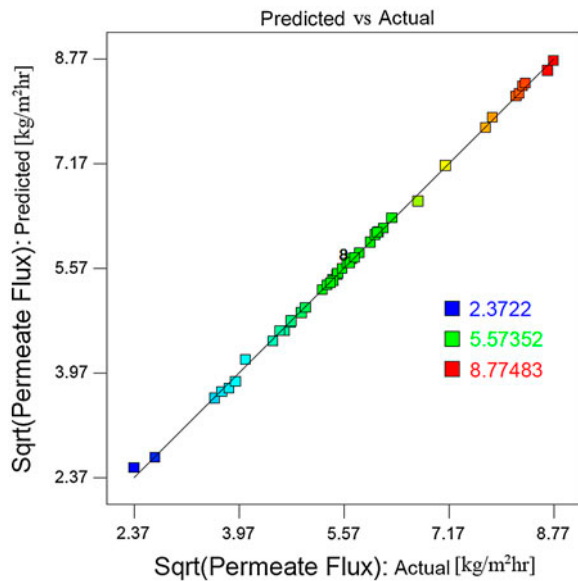


Fig. 6. Plot of experimental vs. predicted response for square root of Permeate flux.

performed to give a better standard error (deviation) and better Adjusted  $R^2$ . The summary of the fit output reports generated by Design-Expert suggested that the quadratic regression model was suitable to explain the relationships between the input variables (feed temperature, coolant temperature, feed flow rate, coolant flow rate, and air gap width) and the output (permeate flux). Therefore, it has been utilized for further analysis. The RSM model ANOVA which summarizes the tests performed for permeate flux is presented in Table 5. The response was consequently expressed in the form of regression equation (response surface model) as follows:

$$\begin{aligned} \text{Square root (Permeate flux)} &= -16.99621 + 0.64355 \times A - 0.15238 \times B \\ &+ 0.30934 \times C + 0.077388 \times D - 0.31755 \times E \\ &+ 0.00152015 \times A \times B - 0.00417221 \times A \times C \\ &- 0.013119 \times A \times E + 0.00330882 \times B \times C \\ &- 0.00686617 \times B \times E + 0.018839 \times C \times E \\ &- 0.00344643 \times A^2 + 0.080799 \times E^2 \end{aligned} \quad (3)$$

where  $A$  is the feed temperature ( $^{\circ}\text{C}$ ),  $B$  is the coolant temperature ( $^{\circ}\text{C}$ ),  $C$  is the feed flow rate (L/min),  $D$  is the coolant flow rate (L/min), and  $E$  is the air gap width (mm). According to ANOVA test results in Table 5, the model has  $F$ -value of 2,118.47, which indicates that the model is significant. The  $p$ -value of  $<0.0001$  implies that there is only a 0.01% chance that a “Model  $F$ -value” this large could occur due to noise.

For significance at 95% confidence level (meaning factors with  $p$ -value  $< 0.0500$  are significant, and those greater than 0.0500 are not significant), the first-order terms ( $A, B, C, D, E$ ), the pairwise interactions terms ( $AB, AC, AE, BC, BE, CE$ ), and quadratic terms ( $A^2$  and  $E^2$ ) are the significant model terms. Other terms in the ANOVA test table are insignificant, and are omitted from the RS-model equation.

From Table 5, it can be observed that the model has an adjusted  $R^2$  of 99.88%, which means that 99.88% of variation in permeate flux is captured by variation in feed temperature, coolant temperature, feed flow rate, coolant flow rate, and air gap width, taking into account the experimental data size and number of independent variables. The model also has standard deviation estimate of 0.049, which measures the variation in the observed permeate flux ( $J$ ) from the regression line. The model predicted  $R^2$  (which measures how accurate the model predicts a response) is 99.79%. This is in agreement with the adjusted  $R^2$  value of 99.88%. The model also has adequate precision of 195.02, which measures the range in predicted response relative to its corresponded error. The model has PRESS value of 0.26. PRESS value is an overall measurement of the discrepancy between the data and the estimation model. The lower the discrepancy, the better the model’s estimations will be.

The coefficients terms of the RS model equation show that the feed temperature has the largest positive effect on permeate flux, while the air gap width gives the greater negative contribution to the flux. Feed and coolant flow rates have positive influences to the model, while the contribution of coolant temperature to the model is negative.

To provide a better understanding of the interaction effect of variables on AGMD parameters, three and two-dimensional plots (Response surface and contour lines plots) for the measured response are generated based on the quadratic RS model equation, Eq. (3). The plots are depicted in Figs. 7–12, where  $T_f, T_c, Q_f, Q_c$ , and  $B$  in the figures represent feed temperature, coolant temperature, feed flow rate, coolant flow rate, and air gap width, respectively. The impact of coolant and feed temperatures on permeate flux are presented in Fig. 7. It can be observed that increasing the feed temperature leads to quadratic increment in system flux. This can be attributed to the exponential relation between vapor pressure and temperature. The flux production decreases almost linearly with increasing coolant temperature, due to reduction in the transmembrane driving force responsible for flux permeation. Fig. 8 shows the influence of feed flow rate and feed temperature on the system productivity. The flux increase with increasing feed temperature (as

Table 5  
ANOVA for response (Permeate flux) surface quadratic model

Source	Sum of squares	df	Mean square	F-value	p-value Prob. > F
Model	102.82	20	5.14	2,118.47	<0.0001
A-feed temperature	49.73	1	49.73	20,491.07	<0.0001
B-coolant temperature	4.21	1	4.21	1,734.72	<0.0001
C-feed flow rate	5.13	1	5.13	2,113.51	<0.0001
D-coolant flow rate	0.2	1	0.2	83.91	<0.0001
E-air gap width	40.1	1	40.1	16,524.76	<0.0001
AB	0.18	1	0.18	76.18	<0.0001
AC	0.22	1	0.22	91.81	<0.0001
AD	9.51E-03	1	9.51E-03	3.92	0.0573
AE	2.2	1	2.2	907.76	<0.0001
BC	0.035	1	0.035	14.44	0.0007
BD	1.60E-03	1	1.60E-03	0.66	0.4239
BE	0.15	1	0.15	62.16	<0.0001
CD	1.90E-03	1	1.90E-03	0.78	0.3837
CE	0.18	1	0.18	74.88	<0.0001
DE	7.80E-03	1	7.80E-03	3.21	0.0835
A <sup>2</sup>	0.29	1	0.29	120.51	<0.0001
B <sup>2</sup>	1.89E-05	1	1.89E-05	7.80E-03	0.9302
C <sup>2</sup>	5.67E-05	1	5.67E-05	0.023	0.8796
D <sup>2</sup>	8.39E-05	1	8.39E-05	0.035	0.8538
E <sup>2</sup>	0.26	1	0.26	106.97	<0.0001
Residual	0.07	29	2.43E-03		
Lack of fit	0.07	22	3.20E-03		
Pure error	0	7	0		
Cor total	102.89	49			
Std. dev.	0.049	R <sup>2</sup>	0.9993		
Mean	5.72	Adj. R <sup>2</sup>	0.9988		
C.V. %	0.86	Pred. R <sup>2</sup>	0.9979		
Press	0.26	Adeq. precision	195.02		

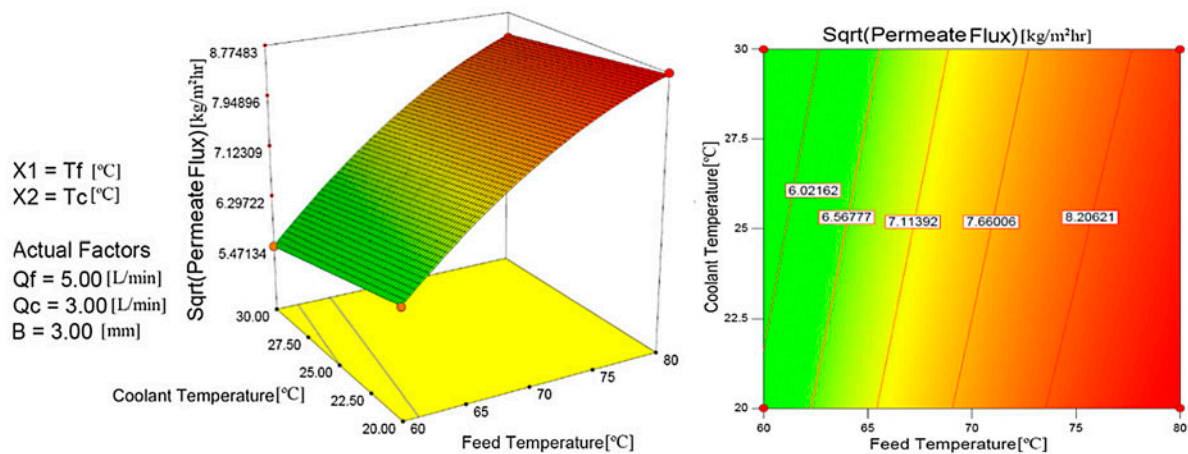


Fig. 7. Response surface plot and contour lines showing the effect of coolant temperature and feed temperature on Sqrt (Permeate flux).

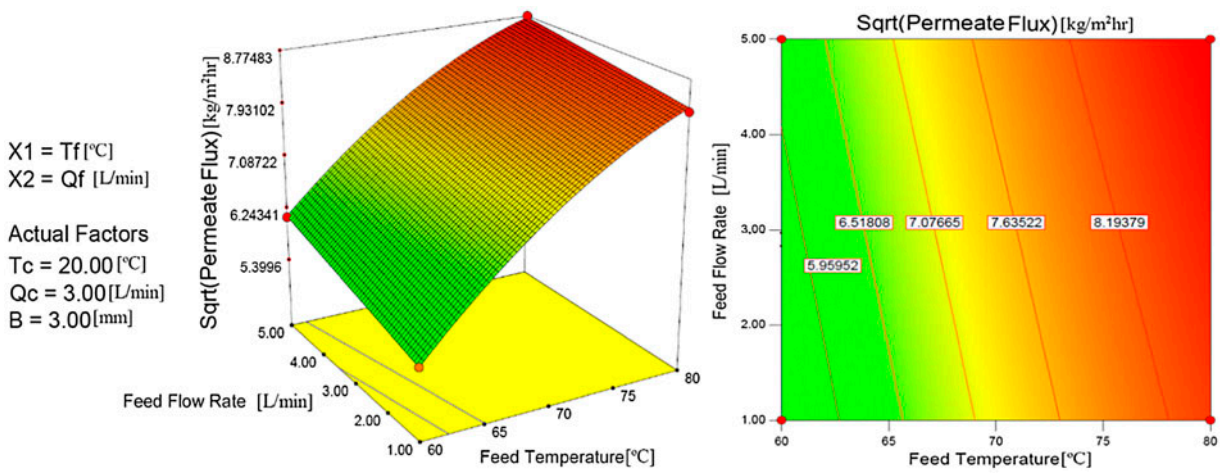


Fig. 8. Response surface plot and contour lines showing the effect of feed flow rate and feed temperature as a function of Sqrt (Permeate flux).

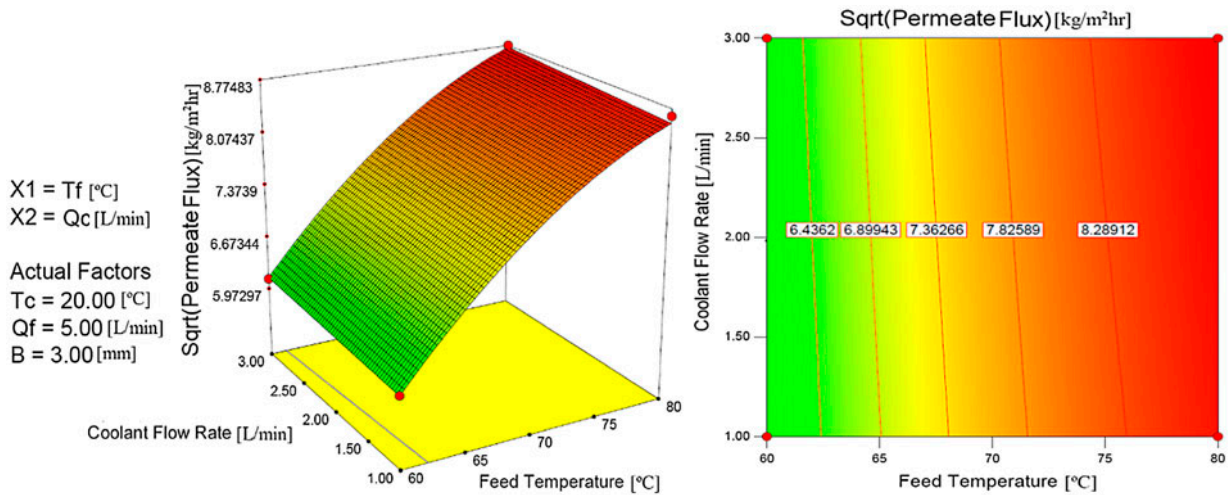


Fig. 9. Response surface plot and contour lines showing the effect of coolant flow rate and feed temperature on Sqrt (Permeate flux).

shown earlier in Fig. 7), and also increase linearly with increasing feed flow rate, due to enhanced turbulence level in the flow channel, and improved heat transfer coefficient in the feed boundary layer. Fig. 9 illustrates the impact of coolant flow rate and feed temperature on the permeate flux. It can be observed that increasing the coolant flow rate leads to a marginal rise in the flux production. This observation indicates that the coolant flow rate is not a significant factor influencing the performance of AGMD process. The effect of the coolant flow rate is insignificant when

compared to other factors; however, it is advisable to include it in the model as suggested by the Design-Expert software. The variations in air gap width with feed temperature, feed flow rate, and coolant temperature as a function of response are shown in Figs. 10–12. As noticed from the figures, decreasing the air gap width from 7 to 3 mm led to a quadratic increment in the permeate flux through the membrane. Decreasing the air gap width means reducing the resistance to mass transfer by reducing the vapor diffusion path length within the air gap compartment

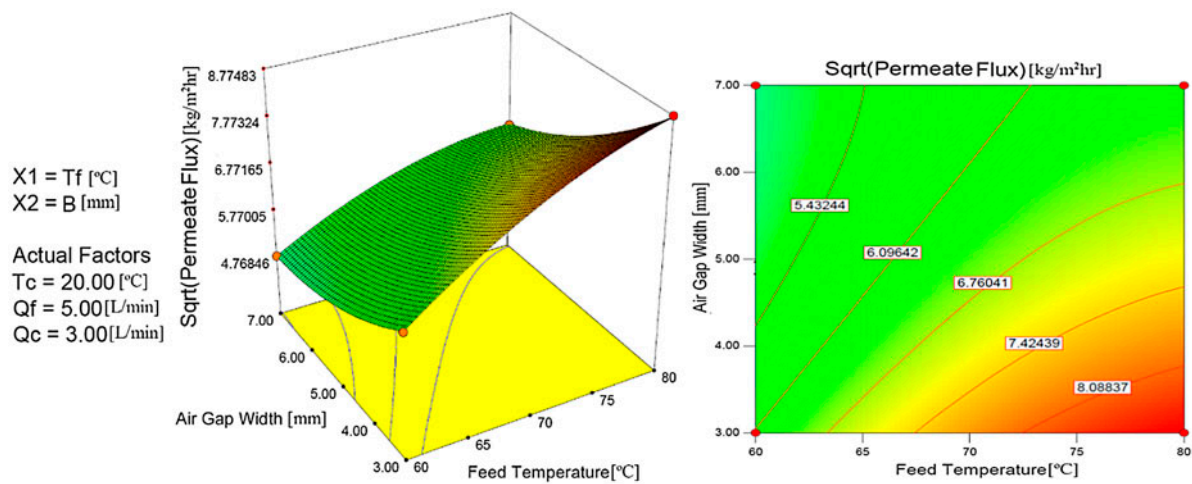


Fig. 10. Response surface plot and contour lines showing the effect of air gap thickness and feed temperature as a function of  $\sqrt{\text{Permeate flux}}$ .

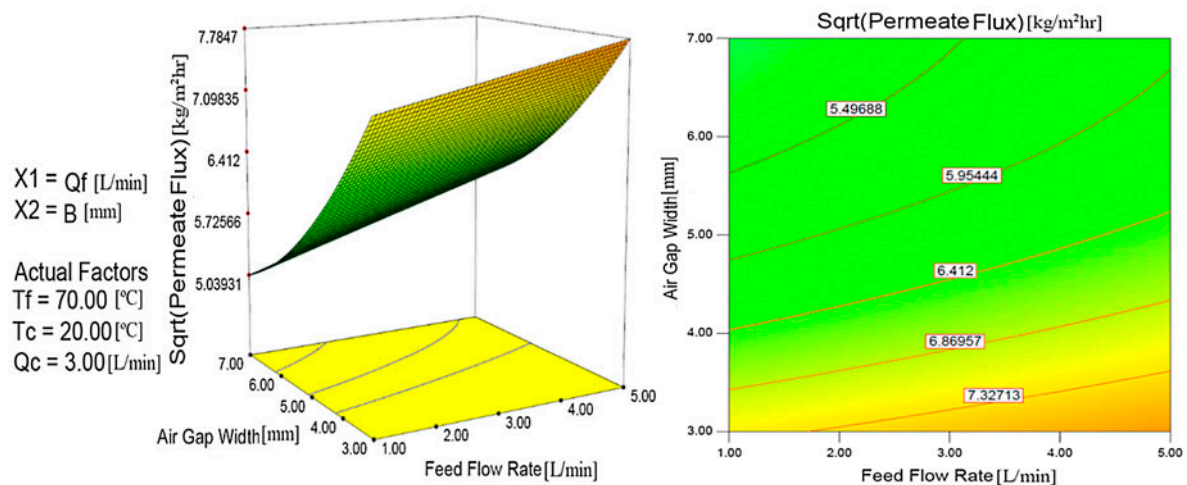


Fig. 11. Response surface plot and contour lines showing the effect of air gap thickness and feed flow rate on  $\sqrt{\text{Permeate flux}}$ .

and increased the driving transmembrane potential. It can be concluded from the above-mentioned figures that both feed temperature and air gap width are the most dominant and strongest factors controlling the system performance. The graphs of other interaction effect of variables on AGMD process (not shown) portray similar trends to the presented figures.

The AGMD system operating parameters were further numerically optimized and the results are presented in Fig. 13. In numerical optimization, one can maximize, minimize, target a single response, target a single response subjected to upper and/or lower

boundaries on other responses, and combinations of two or more responses. The plots obtained for numerical optimization are the ramp function graph, and the desirability bar graph. Ramp function graph for the permeate flux is shown in Fig. 13(a). Ramp function graphs presents the value of parameters that obtain maximum value of permeate flux for different system operating conditions. The function combines the individual graphs for easier interpretation. The dot on each ramp reflects the factor setting or response prediction for that solution. The height of the dot indicates how desirable the factor settings are. Fig. 13(b)

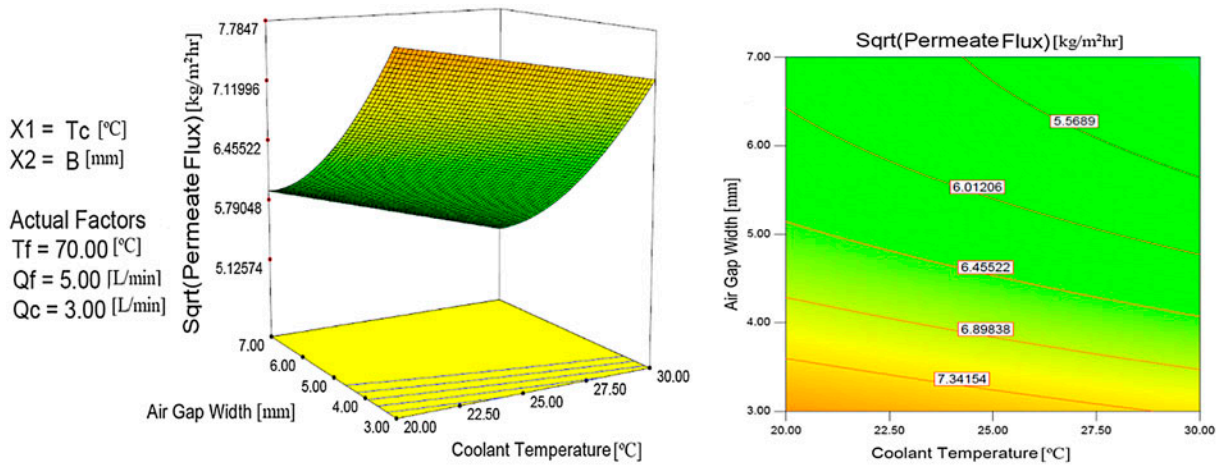


Fig. 12. Response surface plot and contour lines showing the effect of air gap thickness and coolant temperature as a function of Sqrt (Permeate flux).

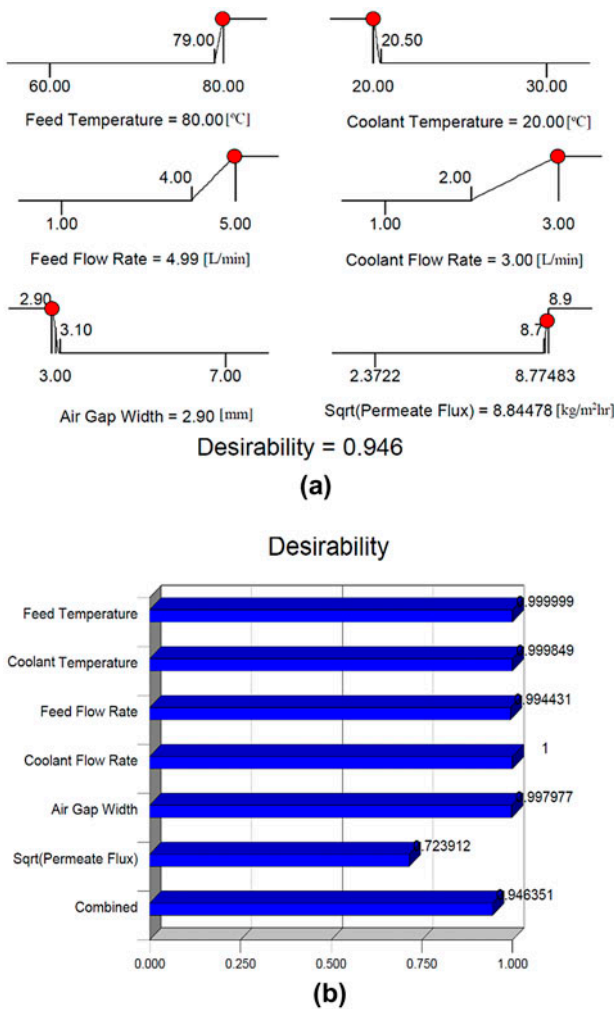


Fig. 13. (a) Ramp function graph, (b) Desirability bar graph on numerical optimization for permeate flux.

presents the desirability bar graph. The program combines the individual desirability's into a single number and then searches for the greatest overall desirability. The program uses five possibilities for a "Goal" to construct desirability indices ( $d_i$ ). The goals are; maximize, minimize, target, in range, and, equal to (factors only) [40]. In our own case, we need to increase the permeate flux, so our goal is flux maximization. Desirability range from zero to one for any given response, and a desirability value of one represents the ideal case, while that of zero indicates that one or more responses fall outside desirable limits. The obtained desirability plots show conflicting optimum factor levels for response. While the feed temperature, feed flow rate, and coolant flow rate need to be maximized, the coolant temperature, and air gap thickness need minimization in order to obtain a desired optimum permeate flux. It can be noticed that the obtained overall desirability is 0.945, which is sufficient for the numerical optimization.

#### 4.3. Confirmation test

In order to verify the adequacy of the generated RS model, the model was validated against the experimental data of RSM design data in Table 4. Furthermore, eight other confirmatory experiments whose variables combinations were not included in RSM design matrix (Table 4) were selected from Table 2 (Taguchi design arrays). The predicted values and the actual experimental data are presented in Table 6. The maximum percentage deviation between the actual and predicted data was 6.34%. This showed

Table 6  
Confirmation experiments

Feed temp. (°C)	Coolant temp. (°C)	Feed flow rate (L/min)	Coolant flow rate (L/min)	Air gap (mm)	Experimental permeate flux (kg/m <sup>2</sup> h)	Predicted permeate flux (kg/m <sup>2</sup> h)	Percentage difference (%)
60	25	3	2	3	28.74353	28.090646	2.324204024
60	25	3	2	7	14.18849	13.342305	6.342123316
60	30	5	3	3	29.93561	29.617723	1.073301261
70	30	1	2	3	42.99345	41.938208	2.516182456
70	20	3	3	3	55.23912	55.934901	1.24391213
70	25	5	1	3	54.02487	53.985731	0.072499651
80	20	5	2	5	52.70894	50.664429	4.035396826
80	20	5	2	3	76.19558	74.744805	1.940970851

that the model gives good predictions of the experimental data. Hence, the generated RS model, which is based on the statistical test, is adequate for flux predictions in AGMD system within the domain of the consider range of parameters.

## 5. Conclusions

The performance of AGMD process was successfully optimized, modeled, and expressed in terms of regression models. The Taguchi and RSM techniques were applied to optimize and investigate the influences of different operating parameters (feed temperature, coolant temperature, feed flow rate, coolant flow rate, and air gap width) on AGMD performance.

The following summaries can be drawn from the presented results:

- (1) Both Taguchi technique and RSM method have shown that all the operating factors except coolant flow rate significantly influences the permeate flux. Both techniques also reveal that feed temperature and air gap width are the most significant factors controlling the performance of AGMD process, with feed temperature portraying the strongest contribution.
- (2) The developed empirical RS model was adequate in explaining the effect of controlling parameters on response. Confirmation experiments showed that the maximum percentage deviation between actual experimental and predicted data was 6.34%.
- (3) According to Taguchi orthogonal experimental design matrix, the optimum control factors combinations are: feed temperature of 80°C, coolant temperature of 20°C, feed flow rate of 5 L/min, coolant flow rate of 2 L/min, and air gap thickness of 3 mm. This combination gave a maximum flux of 76.0457 kg/m<sup>2</sup> h.

- (4) According to RSM-FCCD experimental design matrix, the optimized control factors combinations for permeate flux are: feed temperature of 80°C, coolant temperature of 20°C, feed flow rate of 5 L/min, coolant flow rate of 3 L/min, and air gap thickness of 3 mm. This combination resulted in a maximum flux of 76.99769 kg/m<sup>2</sup> h.
- (5) The RSM showed the significance of all possible combinations of interactions and square terms. The RSM was found to be effective in the identification and development of significant relationships between operating parameters.
- (6) RSM technique can model the interactions and square terms responses of all parameters. This tool is not available in Taguchi technique.
- (7) While RSM technique provides 3-D plots which helps in better visualization and understanding of the effect of operating parameters on response, the Taguchi technique only provides the mean effect plots of response at given level of parameters. RSM also provides desirability bar graphs and ramp function graphs, which provides the exact levels of factors for a desired level of response.
- (8) RSM technique was found to be successful in performing trend analysis of permeate flux in AGMD process with respect to various combinations of design variables.
- (9) The time taken to conduct RSM experiments almost doubled that of Taguchi methodology.

Although both techniques gave very similar results, the optimum flux obtained using RSM techniques is slightly higher than that of Taguchi methodology. The RSM is a better tool for the optimization of AGMD system when compared to Taguchi methodology.

## Acknowledgment

The authors would like to acknowledge the support received from King Fahd University of Petroleum & Minerals (KFUPM) to complete this work under the funded project # IN141035.

## References

- [1] A.C. Sun, W. Kosar, Y. Zhang, X. Feng, Vacuum membrane distillation for desalination of water using hollow fiber membranes, *J. Membr. Sci.* 455 (2014) 131–142.
- [2] J.P. Mericq, S. Laborie, C. Cabassud, Vacuum membrane distillation of seawater reverse osmosis brines, *Water Res.* 44 (2010) 5260–5273.
- [3] Available from: <<http://idadesal.org/desalination-101/desalination-by-the-numbers/>> (accessed on 01 May 2016).
- [4] Y. Wu, Y. Kong, J. Liu, J. Zhang, J. Xu, An experimental study on membrane distillation-crystallization for treating waste water in taurine production, *Desalination* 80 (1991) 235–242.
- [5] V. Calabrò, E. Drioli, F. Matera, Membrane distillation in the textile wastewater treatment, *Desalination* 83 (1991) 209–224.
- [6] F.A. Banat, J. Simandl, Removal of benzene traces from contaminated water by vacuum membrane distillation, *Chem. Eng. Sci.* 51 (1996) 1257–1265.
- [7] A.M. Urriaga, E.D. Gorri, G. Ruiz, I. Ortiz, Parallelism and differences of pervaporation and vacuum membrane distillation in the removal of VOCs from aqueous streams, *Sep. Purif. Technol.* 22–23 (2001) 327–337.
- [8] N. Couffin, C. Cabassud, V. Lahoussine-Turcaud, A new process to remove halogenated VOCs for drinking water production: Vacuum membrane distillation, *Desalination* 117 (1998) 233–245.
- [9] V. Calabro, B.L. Jiao, E. Drioli, Theoretical and experimental study on membrane distillation in the concentration of orange juice, *Ind. Eng. Chem. Res.* 33 (1994) 1803–1808.
- [10] S. Kimura, S. Nakao, Transport phenomena in membrane distillation, *J. Membr. Sci.* 33 (1987) 285–298.
- [11] A.O. Imdakm, M. Khayet, T. Matsuura, A Monte Carlo simulation model for vacuum membrane distillation process, *J. Membr. Sci.* 306 (2007) 341–348.
- [12] A. Alkhudhiri, N. Darwish, N. Hilal, Membrane distillation: A comprehensive review, *Desalination* 287 (2012) 2–18.
- [13] D.U. Lawal, A.E. Khalifa, Flux predictions in direct contact membrane distillation, *Int. J. Mater. Mech. Manuf.* 2(4) (2014) 302–308.
- [14] A. Khalifa, Water and air gap membrane distillation for water desalination—An experimental comparative study, *Sep. Purif. Technol.* 141 (2015) 276–284.
- [15] L. Francis, N. Ghaffour, A. Alsaadi, G. Amy, Material gap membrane distillation: A new design for water vapor flux enhancement, *J. Membr. Sci.* 448 (2013) 240–247.
- [16] M. Essalhi, M. Khayet, Application of a porous composite hydrophobic/hydrophilic membrane in desalination by air gap and liquid gap membrane distillation: A comparative study, *Sep. Purif. Technol.* 133 (2014) 176–186.
- [17] D.U. Lawal, A.E. Khalifa, Experimental investigation of an air gap membrane distillation unit with double-sided cooling channel, *Desalin. Water Treat.* 57(24) (2016) 11066–11080.
- [18] R. Bahar, M.N.A. Hawlader, T.F. Ariff, Channeled coolant plate: A new method to enhance freshwater production from an air gap membrane distillation (AGMD) desalination unit, *Desalination* 359 (2015) 71–81.
- [19] R. Tian, H. Gao, X.H. Yang, S.Y. Yan, S. Li, A new enhancement technique on air gap membrane distillation, *Desalination* 332 (2014) 52–59.
- [20] H. Geng, H. Wu, P. Li, Q. He, Study on a new air-gap membrane distillation module for desalination, *Desalination* 334 (2014) 29–38.
- [21] E. Guillén-Burrieza, G. Zaragoza, S. Miralles-Cuevas, J. Blanco, Experimental evaluation of two pilot-scale membrane distillation modules used for solar desalination, *J. Membr. Sci.* 409–410 (2012) 264–275.
- [22] D. Winter, J. Koschikowski, M. Wiegand, Desalination using membrane distillation: Experimental studies on full scale spiral wound modules, *J. Membr. Sci.* 375 (2011) 104–112.
- [23] A. Ruiz-Aguirre, D.C. Alarcón-Padilla, G. Zaragoza, Productivity analysis of two spiral-wound membrane distillation prototypes coupled with solar energy, *Desalin. Water Treat.* 55 (2015) 2777–2785.
- [24] M. Khayet, Membranes and theoretical modeling of membrane distillation: A review, *Adv. Colloid Interface Sci.* 164 (2011) 56–88.
- [25] G. Zuo, G. Guan, R. Wang, Numerical modeling and optimization of vacuum membrane distillation module for low-cost water production, *Desalination* 339 (2014) 1–9.
- [26] T. Mohammadi, P. Kazemi, Taguchi optimization approach for phenolic wastewater treatment by vacuum membrane distillation, *Desalin. Water Treat.* 52 (2014) 1341–1349.
- [27] C.C. Camposeco-Negrete, Optimization of cutting parameters for minimizing energy consumption in turning of AISI 6061 T6 using Taguchi methodology and ANOVA, *J. Cleaner Prod.* 53 (2013) 195–203.
- [28] I. Asiltürk, S. Neşeli, Multi response optimisation of CNC turning parameters via Taguchi method-based response surface analysis, *Measurement* 45 (2012) 785–794.
- [29] S. Mavruz, R.T. Ogulata, Taguchi approach for the optimisation of the bursting strength of knitted fabrics, *Fibres Text East Eur* 18(2) (2010) 78–83.
- [30] T. Mohammadi, M.A. Safavi, Application of Taguchi method in optimization of desalination by vacuum membrane distillation, *Desalination* 249 (2009) 83–89.
- [31] A.E. Khalifa, D.U. Lawal, Performance and optimization of air gap membrane distillation system for water desalination, *Arab. J. Sci. Eng.* 40(12) (2015) 3627–3639.
- [32] R.H. Myers, D.C. Montgomery, C.M. Anderson-Cook, Response surface methodology: Process and Product Optimization Using Designed Experiments, third ed., John Wiley & Sons, Inc., Hoboken, NJ, 2009.
- [33] L. Dai, J. Peng, H. Zhu, Optimization of the process variables for making direct reduced iron by microwave heating using response surface methodology. Second International Symposium on High-Temperature Metallurgical Processing, Wiley-TMS, San Diego, CA, 2011, pp. 101–110.

- [34] R.K. Bhushan, Optimization of cutting parameters for minimizing power consumption and maximizing tool life during machining of Al alloy SiC particle composites, *J. Cleaner Prod.* 39 (2013) 242–254.
- [35] M. Aloufi, T.J. Kazmierski, A response surface modelling approach to performance optimisation of kinetic energy harvesters, *International Journal of Research and Reviews in Computer Science (IJRRCS)*, Special Issue: Simulation, Benchmarking and Modeling of Systems and Communication Networks (April 2011) 1–9.
- [36] Response Surface Design in Minitab, Instruction manuals, viswanathan\_subram\_4. Available from: <<http://www.scribd.com/doc/231927118/Response-Surface-Design-in-Minitab#scribd>>.
- [37] T. Mohammadi, P. Kazemi, M. Peydayesh, Optimization of vacuum membrane distillation parameters for water desalination using Box–Behnken design, *Desalin. Water Treat.* 56(9) (2015) 2306–2315.
- [38] M. Khayet, C. Cojocaru, Air gap membrane distillation: Desalination, modeling and optimization, *Desalination* 287 (2012) 138–145.
- [39] M. Khayet, C. Cojocaru, C.P. García-Payo, Application of response surface methodology and experimental design in direct contact membrane distillation, *Ind. Eng. Chem. Res.* 46 (2007) 5673–5685.
- [40] Design-Expert Software, Version 7, User's Guide, Technical Manual. Stat-Ease Inc., Minneapolis, MN, 2006.